

Fractional spin textures in the frustrated magnet $\text{SrCr}_{9p}\text{Ga}_{12-9p}\text{O}_{19}$

Arnab Sen,^{1,2} Kedar Damle,¹ and Roderich Moessner³

¹Tata Institute of Fundamental Research, 1, Homi Bhabha Road, Mumbai 400005, India

²Department of Physics, Boston University, 590 Commonwealth Avenue, Boston, Massachusetts 02215, USA

³Max-Planck-Institut für Physik komplexer Systeme, 01187 Dresden, Germany

We consider the archetypal frustrated antiferromagnet $\text{SrCr}_{9p}\text{Ga}_{12-9p}\text{O}_{19}$ in its well-known spin-liquid state, and demonstrate that a Cr^{3+} spin $S = 3/2$ ion in direct proximity to a pair of vacancies (in disordered $p < 1$ samples) is cloaked by a spatially extended spin texture that encodes the correlations of the parent spin-liquid. In this spin-liquid regime, the combined object has a magnetic response identical to a classical spin of length $S/2 = 3/4$, which dominates over the small intrinsic susceptibility of the pure system. This fractional-spin texture leaves an unmistakable imprint on the measured ^{71}Ga nuclear magnetic resonance (NMR) lineshapes, which we compute using Monte-Carlo simulations and compare with experimental data.

PACS numbers: 75.10.Jm 05.30.Jp 71.27.+a

$\text{SrCr}_{9p}\text{Ga}_{12-9p}\text{O}_{19}$ (SCGO) is a remarkable magnetic material which does not show any signs of magnetic ordering even at extremely low temperatures $T \sim \Theta_{CW}/100$, where $\Theta_{CW} \approx 500$ K is the so-called Curie-Weiss temperature at which mean-field theory predicts magnetic ordering of its corner-sharing network (Fig 1) of antiferromagnetically coupled Cr^{3+} $S = 3/2$ moments. The original observation[1–3] of this broad regime of spin-liquid behaviour in SCGO led to an intensive study of a series of samples with varying density $x \equiv 1 - p$ of vacancies in the Cr^{3+} spin network, including NMR[4], susceptibility[5], and μSR [6] experiments. Thus, SCGO is among the best known and most systematically studied candidates for spin-liquid behaviour in frustrated magnets.

One key observation, due to Schiffer and Daruka, was the presence of a paramagnetic “Curie tail” in the low temperature uniform susceptibility of these compounds, well modeled by a defect contribution $\chi_{\text{defect}} = C_d/T$ that dominates over the intrinsic susceptibility $\chi_{\text{intrinsic}} \approx C_1/(T + \Theta_{CW})$ for $T \ll \Theta_{CW}$; the Curie constant C_d in this “two-population” phenomenology was associated with a population of paramagnetic objects dubbed “orphan spins” [5]. Another important observation, due originally to Limot *et. al.*[4], is the *apparently symmetric* NMR line broadening ΔH that scales as $\Delta H \propto x/T$ for not-too-low x and T ; this was in turn interpreted phenomenologically as a signature of a disorder-induced spin-texture—a short-ranged oscillating spin density profile induced by some lattice defects.

On the theoretical side, Berlinsky and one of us used a “single-unit approximation”[7] to predict that “defective” simplices (corner-sharing units), in which all but one spin has been substituted for with non-magnetic impurities, must give rise to Curie tails in the low temperature susceptibility of isotropic classical spin- S antiferromagnets on corner-sharing lattices such as SCGO. In related work, Henley used classical energy minimization considerations at $T = 0$ to argue that an infinitesimal

magnetic field applied to such a system with a single defective simplex should induce a spin-texture with saturation magnetization $S/2$ [8]. This suggested that the phenomenological orphan spins[5] and oscillating spin textures[4] invoked earlier are related to the presence of such defective simplices, with the lone spins on such defective simplices providing a microscopic basis for the phenomenological orphan spin population of Ref 5. Although this orphan-texture complex (comprising the orphan spin on a defective simplex and its surrounding spin texture) has thus been implicated in some of the most intriguing experimental observations on SCGO, a fundamental understanding of it has been lacking.

Here, we develop a quantitatively accurate analytical theory that provides a full characterization of this orphan-texture complex by accounting for both entropic and energetic effects in the spin-liquid regime of low temperatures ($\bar{T} \equiv k_B T / JS^2 \ll 1$) and low magnetic field h ($\bar{h} \equiv g_L \mu_B h / JS \ll 1$), but arbitrary \bar{h}/\bar{T} . In this regime, we find that the orphan spin magnetisation is equal to the magnetisation of a spin S in a field $h/2$. This is accompanied by an extended spin-texture, which is scale-free at $T = 0$ but acquires a finite extent as T is increased. We determine the intricate pattern of spin correlations in the texture and demonstrate that its net magnetisation *cancels off half of the orphan spin’s moment*, thus giving rise to an orphan-texture complex that behaves as a *classical spin $S/2$ in field h* , with a susceptibility given by

$$\chi_{S/2}(T) = (g_L \mu_B S/2)^2 / 3k_B T$$

This provides a particularly dramatic instance of fractionalisation of spins in a simple classical system.

In remarkable correspondence with experiment[4], we find that these extended, fractional-spin orphan-texture complexes show up prominently in SCGO at not-too-low $x = 1 - p$ as a large, nearly symmetric low temperature broadening $\Delta H \propto x/T$ of our predictions for the $^{71}\text{Ga}(4f)$ NMR line[4] associated with Ga nuclei at the

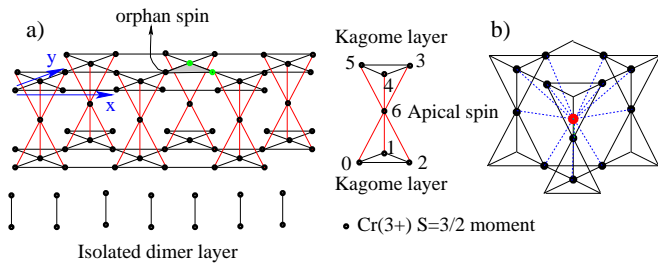


FIG. 1: a) The Cr atoms in SCGO form a lattice made up of kagome bilayers separated from each other by a layer of isolated dimers consisting of pairs of Cr atoms. Each kagome bilayer is a corner sharing arrangement of tetrahedra and triangles made up of two Kagome lattices that are coupled to each other through “apical” Cr sites shared between up-pointing and down-pointing tetrahedra. Links between near-neighbour Cr sites in each bilayer represent a Heisenberg exchange coupling $J = 80$ K between neighbouring Cr^{3+} spins, while links in the isolated dimer layer represent a Heisenberg exchange coupling $J' = 216$ K between the two Cr^{3+} ions that constitute each pair. Two vacancies in a triangle (green circles) leave behind an orphan spin. b) The 12 Cr^{3+} sites (black) that are hyperfine coupled to a given Ga(4f) site (red) in the SCGO lattice.

so-called (4f) crystallographic position in the SCGO lattice (Fig 1). We therefore focus below on this particular case, although our analytical low temperature, low field results apply more generally to orphan-texture complexes surrounding isolated defective simplices in kagome, pyrochlore and SCGO lattices.

SCGO is described by the classical Hamiltonian:

$$\mathcal{H} = \frac{J}{2} \sum_{\boxtimes} \left(\sum_{i \in \boxtimes} \vec{S}_i - \frac{g_L \mu_B \vec{h}}{2J} \right)^2 + \frac{J}{2} \sum_{\Delta} \left(\sum_{i \in \Delta} \vec{S}_i - \frac{g_L \mu_B \vec{h}}{2J} \right)^2$$

where \vec{S}_i are classical length- S spins ($S = 3/2$ for SCGO) with saturation moment $g_L S$ in units of the Bohr magneton μ_B ($g_L = 2$ for SCGO), J is the nearest-neighbour Heisenberg exchange coupling ($J \simeq 80\text{K}$ for SCGO[4]), and \vec{h} is the external field. \boxtimes refers to the tetrahedra that consisting of a triangle in a kagome layer attached to an apical spin in the triangular layer (Fig 1), while Δ refers to those triangles in the kagome layer which are not associated with an apical spin.

Here, we model the pure $p = 1$ system in terms of an effective free energy functional \mathcal{F} that incorporates the energetics of the antiferromagnetic interactions J on an equal footing with entropic effects of thermal fluctuations:

$$\mathcal{F} = \mathcal{H}(\{\vec{\phi}_i\}) + \frac{T}{2} \sum_i \rho_i \vec{\phi}_i^2$$

The unconstrained effective field $\vec{\phi}_i$ serves as a surrogate for the microscopic fixed-length spin variables \vec{S}_i , with the statistical weight of a field configuration $\{\vec{\phi}_i\}$

being proportional to $\exp(-\mathcal{F}/T)$. $\mathcal{H}(\{\vec{\phi}_i\})$ is the classical Hamiltonian of the system now written in terms of $\vec{\phi}_i$, and the phenomenological stiffness constants ρ_i are fixed by requiring that the mean length of $\vec{\phi}_i$ equal S within the effective theory: $\langle \vec{\phi}_i^2 \rangle_{\mathcal{F}} = S^2$ [9]. For a background to this approach for pure systems, see the review by Henley[10].

To incorporate disorder effects in diluted $p < 1$ samples, we assume that the stiffness constants do not change significantly from their pure values, but extend the effective theory in two important ways: First, we model vacancies in the lattice by setting $\vec{\phi}_i$ to zero on vacancy sites. Secondly and more crucially, as the fixed length nature of an orphan spin on a defective simplex is expected to play a central role, we retain it as a microscopic length- S spin and do not introduce an effective field variable at such sites.

We now use this effective theory to analyze the SCGO magnet with a single defective triangle, *i.e.* two vacancies on one triangle of the SCGO lattice (Fig 1). In this case, the effective theory reduces to a length- S orphan spin $S\vec{n}$ ($\vec{n}^2 = 1$) coupled to a constrained Gaussian theory for $\vec{\phi}_i$ (with constraints $\vec{\phi}_i = 0$ at the two vacancy sites). Focusing first on the orphan spin $S\vec{n}$ in this defective triangle by integrating out the $\vec{\phi}$ fields, we find[9] that the exchange field from the surrounding spin liquid “screens” exactly half the external magnetic field on the orphan spin in the low temperature, low field spin liquid regime, yielding a spin S variable that “sees” a magnetic field $h/2$, and therefore develops a polarization equal to that of a free classical spin S in a field $h/2$. This striking prediction is fully confirmed by Monte-Carlo studies[9] of the classical SCGO magnet with one defective triangle (see Fig 2 (a)), which also reveal that this prediction is surprisingly robust, remaining accurate for temperatures as high as $T \sim 0.1JS^2$ for this example.

Next, we turn to a detailed description of the extended spin texture that cloaks this orphan spin in the spin-liquid regime. In addition to the uniform external field $\vec{h} = h\hat{z}$ that acts on all the $\vec{\phi}_i$ in the constrained Gaussian action, this orphan spin polarization also gives rise to a local exchange field that acts in the \hat{z} direction on $\vec{\phi}_i$ at the two undiluted sites adjacent to the orphan spin. The extended spin texture surrounding the orphan spin is modeled within the effective theory by calculating the response $\langle \phi_i^z \rangle_{\mathcal{F}}$ to these fields[9]. At $T = 0$, the computed texture’s envelope decays as $1/|\vec{r}|$ away from the orphan spin, while the overall scale is set by the orphan spin’s saturation magnetization. At finite- T and small fields in the spin-liquid regime, the power law envelope is cut off by a thermally introduced finite correlation length $\xi \sim 1/\sqrt{T}$, endowing it with an effective size $\xi^d \sim 1/T^{d/2}$ in d dimensions; in our $d = 2$ example, this gives a spatial size $\sim 1/T$ scaling identically with the overall magnetization scale of the texture, which is set by the orphan spin’s susceptibility $\sim 1/T$. These predictions are compared

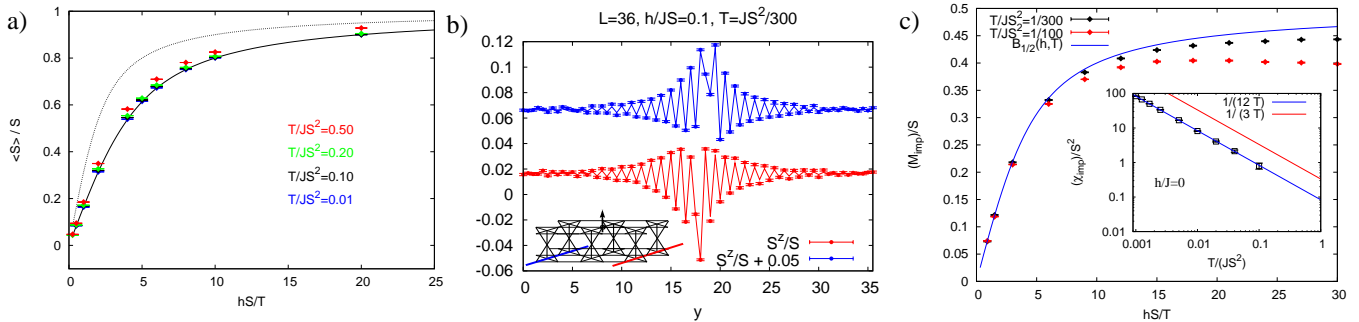


FIG. 2: a) The orphan spin in field h develops magnetization (symbols) that matches that of an isolated spin S in field $h/2$ (full line) in the spin liquid regime. Also shown (dotted curve) is the magnetization expected for an isolated spin S in field h . b) The orphan induced spin texture is shown along two cuts on the lattice. Numerical data is shown as points with statistical error bars and the effective theory result as lines in the main plot. The spin texture shown in red (blue) in main plot is along the cut shown in red (blue) in the inset. The orphan spin is denoted by an arrow in the inset. c) The impurity magnetization (defined as the difference in magnetic response between the diluted and the pure system) of a single orphan-texture complex (symbols) compared with $B_{S/2}(h, T)$ (solid curve), the asymptotic prediction deep in the spin-liquid regime. $B_{S/2}(h, T)$ is the magnetization curve of a classical spin $S/2$. Note the much faster convergence of numerical data to asymptotic predictions in the linear (small hS/T) part of the magnetization curve as compared with the non-linear regime at large hS/T . Inset: The corresponding impurity susceptibility (defined in text) matches the susceptibility of a free classical spin $S/2$ up to remarkably high temperatures $T \sim 0.1JS^2$. All Monte-Carlo data exhibited in a) was extrapolated to the thermodynamic limit using a sequence of sizes up to $L = 36$ (with $7L^2$ sites), while that in c) was extrapolated using a sequence of sizes up to $L = 20$.

with Monte-Carlo simulation[9] results in Fig 2 (b) for the case of a single defective triangle in SCGO, and the agreement is remarkably good.

Although the computed texture decays slowly (as $1/|\vec{r}|$ at $T = 0$), its oscillations conspire to reduce its net moment so that it *cancels out precisely half* of the orphan spin’s moment, endowing the orphan-texture complex with a net “impurity magnetization” (excess magnetization over and above that of a pure system in the same external field) equal to the magnetization of a classical spin $S/2$ in field h . The corresponding “impurity susceptibility” χ_{imp} arising from a single orphan-texture complex is $(g_L \mu_B S/2)^2 / 3k_B T$ —a Curie tail dominating the low- T response. For the case of a single defective triangle in SCGO, our Monte Carlo simulations validate this striking prediction up to surprisingly high temperatures of order $T \sim 0.1JS^2$ (Fig 2 (c)).

Fortunately, this novel physics leaves its imprint on the Ga(4f) NMR line, which is a sensitive probe of the distribution of the twelve Cr spin polarizations that are hyperfine coupled to each Ga(4f) nucleus in SCGO (Fig 1 (b)). We calculate this distribution in diluted SCGO lattices with uncorrelated site dilution probability $x = 1 - p$ [9], using the experimentally known values[4] of these hyperfine couplings, and Monte-Carlo simulations[9] to fully account for the physics of a non-zero density of orphan spins in order to obtain quantitatively accurate results.

As is clear from the example at $x = 0.2$ shown in Fig 3 (a), this calculation predicts a line that is broad and appears symmetric, reflecting the fact that the spin textures are staggered and involve a very large number of spins, making it difficult to discern the $O(1)$ net moment of each

texture that endows the line with a slight bias towards lower magnetic fields.

In Fig 3 (c), we show the temperature and x dependence of the width of our predicted lines for not-too-small values of x and T , of greatest relevance to experiments. As the lineshape is not well-approximated by a Gaussian, we do not fit the line to a Gaussian, but rather use the definition $\Delta H \equiv 2\sqrt{2 \ln(2)} (\langle H^2 \rangle - \langle H \rangle^2)^{1/2}$ which reduces to the standard value for a Gaussian line but provides an unbiased measure of the width in more general cases. As is clear from Fig 3 (b), the theoretical predictions for ΔH have the expected “Curie tail” $\Delta H \sim \mathcal{A}(x)/T$ at low temperature. For uncorrelated site disorder, the coefficient \mathcal{A} is expected to scale as x^2 for asymptotically small x ; however, for not-too-small x relevant to experiment, we find that $\mathcal{A}(x)$ can be fit well by an approximately *linear* x dependence $\mathcal{A}(x) \sim x$.

Thus, our theory reproduces the broad, apparently symmetric lines seen in experiments, with broadening scaling as $\Delta H \sim x/T$ for not-too-low x and T . Although these experimental facts are fully reproduced, we caution that our results do not provide a fully quantitative explanation of the NMR data: As is clear from Fig 3 (b), our minimal disorder model consisting of independent vacancies of the nominal experimental density significantly underestimates the absolute scale of the linewidth ΔH . Since isolated vacancies lead to no oscillating spin textures scaling as $1/T$ [9], this discrepancy clearly demonstrates that the density of orphan spins in the experimental samples is significantly higher than that expected from uncorrelated Ga substitution of the Cr lattice. The most frugal resolution is perhaps that the Ga substitu-

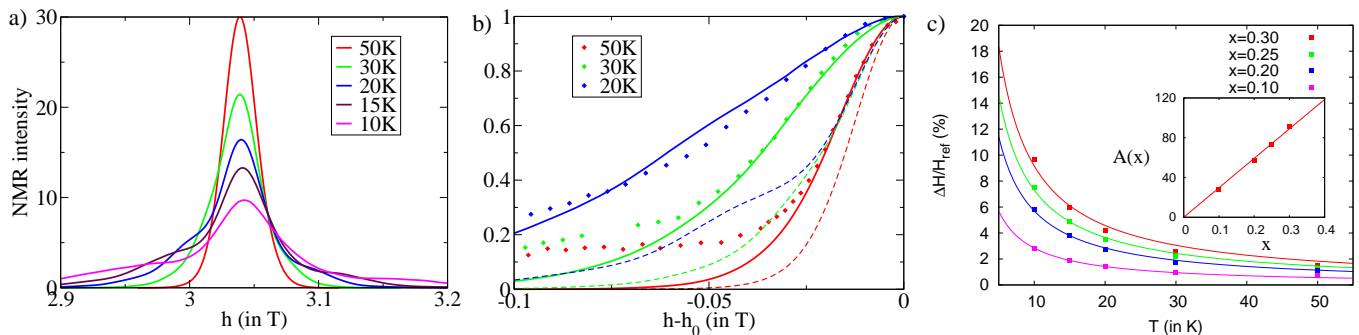


FIG. 3: Predictions for Ga(4f) NMR lines. a) $^{71}\text{Ga}(4f)$ “field-scan” NMR lines predicted within the minimal disorder model of uncorrelated dilution at vacancy density $x = 0.2$. (b) Experimental results of Ref [4] for field-scan $^{71}\text{Ga}(4f)$ NMR lines (dots) at dilution $x = 0.19$, plotted using datafiles provided by P. Mendels, and compared to theoretical predictions of the minimal disorder model (with y axis rescaled and x axis offset appropriately for easy comparison of linewidths and shapes of all curves) at vacancy density $x = 0.2$ (dashed curves) and $x = 0.3$ (full curves). Only the low-field side of the experimental line is compared with theory, as the high-field side of the experimental line is known to be contaminated by the presence of a satellite peak arising from non-stoichiometric (impurity) ^{71}Ga nuclei located at three different Cr sites in the SCGO lattice[4]. (c) Temperature and x dependence of the width ΔH of the theoretically predicted field-scan $^{71}\text{Ga}(4f)$ NMR lines, normalized by a reference field $H_{ref} = 3.12\text{T}$. Solid curves in the main plot are fits of ΔH to $\mathcal{A}(x)/T$ over the experimentally relevant temperature range, and inset shows the approximately linear x dependence of the best-fit values of $\mathcal{A}(x)$ over the experimentally relevant range of x . The Monte-Carlo simulations were performed using a sequence of sizes ranging from $L = 16$ to $L = 50$ (with $7L^2$ sites) to eliminate finite-size effects, with on average 20 disorder realizations at each size.

tion in the Cr kagome layer may be correlated. Additionally, and perhaps more realistically, other sources of disorder, for instance random strain-induced bond randomness, could also affect the effective density of ‘orphan spins’. Unfortunately, it does not seem possible to use measurements of the impurity Curie constant C_d [5] to shed light on this, as uniform susceptibility measurements also pick up, apart from the signal due to Kagome layer orphan spin textures, a much larger “background” contribution from free Cr spins created when Ga impurities substitute for Cr in the isolated dimer layer (Fig 1) of the SCGO lattice.

In conclusion, we note that these disorder induced orphan-texture complexes in SCGO embody several central themes of modern condensed matter physics: The emergence of new types of extended degrees of freedom, and their rich physics at finite density, is a common strand that runs through diverse examples[11] such as Skyrmion lattices in spinor condensates[12], itinerant [13] and quantum Hall magnets[14, 15], and spin textures in topological phases of matter[16]. Moreover, the fact that our textures give rise to a relatively strong magnetic response—their staggered $1/r^{d-1}$ magnetisation profile is *parametrically* stronger than the intrinsic $1/r^d$ spin correlations of the parent spin-liquid—shows that, like in the case of defects evidencing the d-wave nature of the order parameters in the cuprates, imperfections are among the best and most direct probes of exotic correlated states of matter.

The authors thank P. Mendels for providing the orig-

inal NMR data (Fig 3 b) and gratefully acknowledge useful discussions with F. Bert, D. Dhar, C. Henley, P. Mendels, P. Schiffer, and A. Zorko, funding from DST SR/S2/RJN-25/2006, financial support for collaborative visits from the Fell Fund (Oxford), the ICTS TIFR (Mumbai), ARCUS (Orsay) and MPIPES (Dresden), as well as computational resources at TIFR.

-
- [1] X. Obradors *et. al.*, Solid State Commun. **65**, 189 (1988).
 - [2] B. Martinez, A. Labarta, R. Rodriguez-Sola, and X. Obradors, Phys. Rev. B **50** 15779 (1994).
 - [3] A. P. Ramirez, G. P. Espinosa, and A. S. Cooper, Phys. Rev. Lett. **64**, 2070 (1990).
 - [4] L. Limot *et. al.*, Phys. Rev. B **65**, 144447 (2002).
 - [5] P. Schiffer and I. Daruka, Phys. Rev. B **56**, 13712 (1997).
 - [6] Y. J. Uemura *et. al.*, Phys. Rev. Lett. **73**, 3306 (1994).
 - [7] R. Moessner and A. J. Berlinsky, Phys. Rev. Lett. **83**, 3293 (1999).
 - [8] C. L. Henley, Can. J. Phys. **79**, 1307 (2001).
 - [9] A. Sen, K. Damle, and R. Moessner, unpublished.
 - [10] C. L. Henley, arXiv:0912.4531, unpublished (2009).
 - [11] C. Day, Physics Today, **62**, 12 (2009).
 - [12] R. W. Cherng, *Ph.D. thesis* (Harvard University, 2009).
 - [13] S. Mühlbauer *et. al.*, Science **323** 915 (2009).
 - [14] S. Sondhi, A. Karlhede, S. A. Kivelson, and E. H. Rezayi, Phys. Rev. B **47**, 16419 (1993).
 - [15] G. Gervais *et. al.*, Phys. Rev. Lett. **94**, 196803-1 (2005).
 - [16] D. Hsieh *et. al.*, Science **323** 919 (2009).